Ionic liquid gating of single-walled carbon nanotube devices with ultra-short channel length down to 10 nm

Alexander Janissek, Jakob Lenz, Fabio del Giudice, et al.

View Online   Export Citation   CrossMark

ARTICLES YOU MAY BE INTERESTED IN
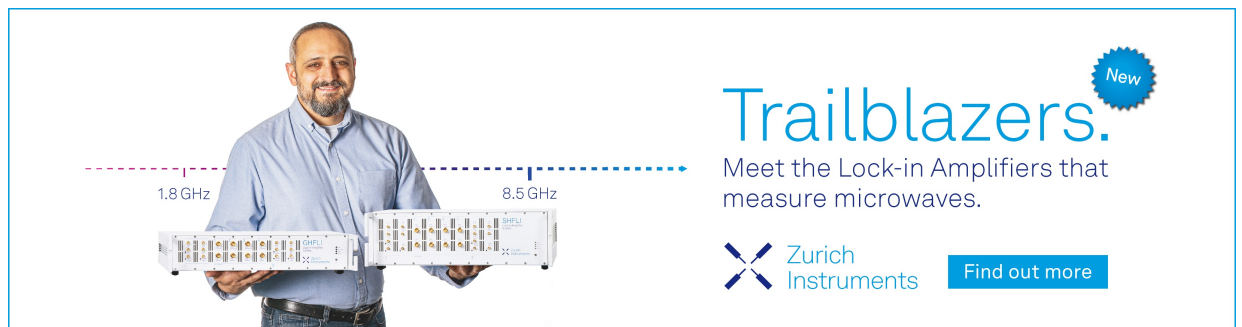
Raman spectroscopy for carbon nanotube applications
Journal of Applied Physics **129**, 021102 (2021); https://doi.org/10.1063/5.0030809

Opportunities for ionic liquid/ionogel gating of emerging transistor architectures
Journal of Vacuum Science & Technology B **39**, 011001 (2021); https://doi.org/10.1116/6.0000678

Charge transport in semiconducting carbon nanotube networks
Applied Physics Reviews **8**, 041318 (2021); https://doi.org/10.1063/5.0065730

Ionic liquid gating of single-walled carbon nanotube devices with ultra-short channel length down to 10 nm

Alexander Janissek,[1,2] (iD) Jakob Lenz,[3] Fabio del Giudice,[3] Marco Gaulke,[1,2] (iD) Felix Pyatkov,[1] Simone Dehm,[1] Frank Hennrich,[1,4] Li Wei,[5] Yuan Chen,[5] (iD) Artem Fediai,[1,a)] Manfred Kappes,[1,4,6] Wolfgang Wenzel,[1] (iD) Ralph Krupke,[1,2,4,a)] (iD) and R. Thomas Weitz[3,7,a)] (iD)

AFFILIATIONS

[1]Institute of Nanotechnology, Karlsruhe Institute of Technology, 76021 Karlsruhe, Germany
[2]Institute of Materials Science, Technische Universität Darmstadt, 64287 Darmstadt, Germany
[3]AG Physics of Nanosystems, Faculty of Physics, Ludwig-Maximilians-University Munich, Geschwister-Scholl-Platz 1, 80539 Munich, Germany
[4]Institute for Quantum Materials and Technologies, Karlsruhe Institute of Technology, 76021 Karlsruhe, Germany
[5]School of Chemical and Biomolecular Engineering, The University of Sydney, Sydney, New South Wales 2006 Australia
[6]Institute of Physical Chemistry, Karlsruhe Institute of Technology, 76128 Karlsruhe Germany
[7]1st Institute of Physics, Faculty of Physics, Georg-August-University, Friedrich-Hund-Platz 1, 37077 Göttingen, Germany

[a)]Authors to whom correspondence should be addressed: krupke@kit.edu; thomas.weitz@uni-goettingen.de; and artem.fediai@kit.edu

ABSTRACT

Ionic liquids enable efficient gating of materials with nanoscale morphology due to the formation of a nanoscale double layer that can also follow strongly vaulted surfaces. On carbon nanotubes, this can lead to the formation of a cylindrical gate layer, allowing an ideal control of the drain current even at small gate voltages. In this work, we apply ionic liquid gating to chirality-sorted (9, 8) carbon nanotubes bridging metallic electrodes with gap sizes of 20 nm and 10 nm. The single-tube devices exhibit diameter-normalized current densities of up to 2.57 mA/μm, on-off ratios up to 10^4, and a subthreshold swing down to 100 mV/dec. Measurements after long vacuum storage indicate that the hysteresis of ionic liquid gated devices depends not only on the gate voltage sweep rate and the polarization dynamics but also on charge traps in the vicinity of the carbon nanotube, which, in turn, might act as trap states for the ionic liquid ions. The ambipolar transfer characteristics are compared with calculations based on the Landauer–Büttiker formalism. Qualitative agreement is demonstrated, and the possible reasons for quantitative deviations and possible improvements to the model are discussed. Besides being of fundamental interest, the results have potential relevance for biosensing applications employing high-density device arrays.

Single-walled carbon nanotubes have been a subject of study for nearly three decades, and over 20 years have passed since the first carbon nanotube transistor had been reported by Tans *et al.*[1] Since then, research in the field of carbon nanotube electronics has explored the potential of both high-performance and thin-film transistors,[2] and with the recent realization of the first carbon nanotube-based microprocessor,[3] the vision of carbon nanotubes replacing silicon seems to be within reach. As in classical silicon electronics, reducing the channel length of a carbon nanotube transistor enhances the

device performance, and sub-10 nm channel lengths have been demonstrated in solid-state devices.[4,5] One of the challenges in making ultra-short channel devices is the fabrication of the gate dielectric and electrode in closest proximity.

A rather simple, low-cost approach is employing liquid gating, where the double layer that forms on any surface is subjected to an electrolyte that functions as an insulating layer appropriate for electric field gating.[6–8] A disadvantage of liquid gating is the inherently low ion mobility in electrolytes, which makes liquid gated devices not

suitable for high-frequency transistors. Consequently, the cutoff frequency of electrolyte gated organic transistors is currently limited to the kHz regime[8,9] and even the predicted 10 MHz[10] is far below the 100 GHz[11,12] operation shown for solid gated CNT transistors. However, for ultra-low power operation devices[13] and for biological and chemical sensing applications, where the response time is less demanding, liquid gating—in particular, in water-based electrolytes—is of great interest.[14] Also, the usage of a hydrogen-doped poly(ethylene glycol) monomethyl ether gated CNT transistor as an artificial synapse was already realized.[15] Several groups have demonstrated liquid gating as an effective way of gating carbon nanotubes using a range of different electrolytes, such as NaCl,[16,17] KCl,[18] PEO/LiClO$_4$ polymer,[19] and phosphate buffer.[20–23] More recently, ion gels consisting of the ionic liquid [EMIM][FAP] and a fluorinated polymer were also used.[24] Ionic liquids and gels have the great advantage that their vapor pressure is negligible, and as molten salts, their screening length is expected to be on the scale of the ionic radii and, hence, sub-nanometer.

While these existing works took advantage of the large capacitance and nanoscopic dimension of the ionic double layer, a reduction in the source/drain dimensions—i.e., the other critical parameter for transistor miniaturization—has not been tested extensively. In this work, we consequently investigate ionic liquid gated ultra-short channel transistor devices with source-drain separations down to 10 nm, which—as we show—exhibit superior electrical characteristics. Since the experiments were performed with mono-chiral (9, 8) carbon nanotubes, and due to the short channel length of the devices, a direct comparison with a

rather simple model calculation based on the Landauer–Büttiker formalism for a ballistic carbon nanotube is possible; this lays the basis for future in-silico optimization of device parameters.

Our nanotubes were produced by a selective catalytic CVD method,[25,26] dispersed in toluene by wrapping in poly(9,9-di-n-dodecylfluorenyl-2,7-diyl) (PFD), and purified and length sorted by gel filtration. For details, we refer to Refs. 27 and 28. The absorption spectrum in Fig. 1(a) gives evidence for a high content of (9,8) nanotubes and the presence of (8,7), (9,7), (10,8), and (10,9) species in minor concentrations in the dispersion. To comply with the nominal charge transfer length for side-contacted nanotubes,[29] fractions of length-sorted (9,8) nanotubes were selected for depositions such that nanotubes were at least 200 nm longer than the distance between the source-drain electrodes. Mono-chiral (9, 8) nanotube transistors with Pd source-drain electrodes were fabricated on 300 nm SiO$_2$/p-doped Si substrates by electron-beam lithography, metallization, and simultaneous electric field site-selective-assisted deposition of single nanotubes (dielectrophoresis),[27] as illustrated schematically in Figs. 1(b) and 1(c). A representative contact with a gap size of 20 nm before nanotube deposition is shown in Fig. 1(e). Since scanning electron imaging before measurements is not advisable and after the application of the ionic liquid not possible, we refer for images with nanotubes to comparable devices shown in Ref. 27.

The electrochemical window given by the anodic and cathodic limits is defined as the difference between the reduction and oxidation potential of anions and cations, respectively. Here, an increasing water
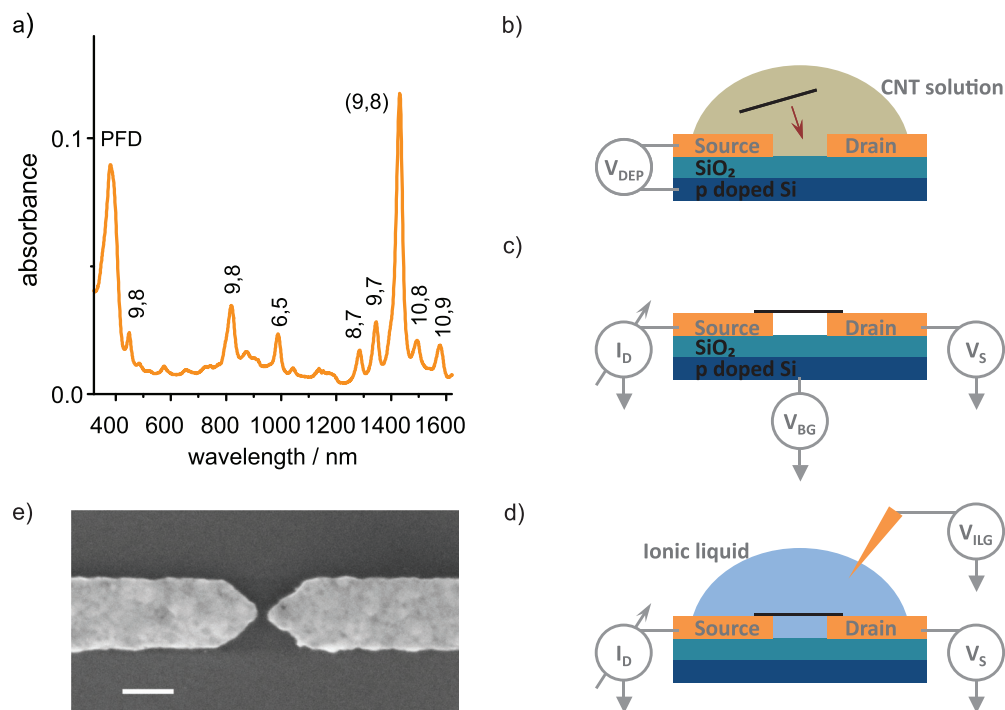

FIG. 1. (a) Absorption spectrum of length-fractionated, PFD-polymer wrapped carbon nanotubes dispersed in toluene containing mainly the (9, 8) chirality. (b) Deposition of CNTs from the dispersion by dielectrophoresis at bias voltage V_{DEP} onto Pd electrodes/300 nm-SiO$_2$/p-Si. After CNT deposition, the sample was rinsed with toluene. (c) and (d) Measurement of drain current (I_D) vs source bias (V_S) and ionic liquid gate voltage (V_{ILG}). (e) Scanning electron micrograph of a device before nanotube deposition. The gap size between Pd electrodes is 20 nm. The scalebar is 100 nm.

content results in narrowing of the electrochemical window at both the cathodic and anodic limits, which is most likely caused by water electrolysis.[30] Depending on the water content, different anodic and cathodic limits for [EMIM][TFSI] can be found in the literature. For 24 h 333 K vacuum dried samples (H_2O content 105 ppm), O'Mahony et al.[31] measured -2.2 V (-2.4 V) as the cathodic limit and 2 V (2.2 V) as the anodic limit vs an fc/fc$^+$ reference electrode at a current density of 1 mA/cm^2 (5 mA/cm^2). For an H_2O content of 3385 ppm in an ambient atmosphere, the cathodic limit reduces to -1.2 V (-2 V) and the anodic limit to 1.6 V (1.7 V). In a different approach where the ionic liquid is dried with sparging N_2 (no water content given), the cathodic and anodic limit vs an Ag/AgCl reference electrode is -2.07 V and 2.2 V.[32] For the liquid gating in our experiments, a small drop of the ionic liquid 1-ethyl-3-methylimidazolium bis(trifluoromethylsulfonyl)imide [EMIM][TFSI] was placed on top of the sample. To reduce the water content, our samples were stored for 12 h at 50 °C and 5 mbar in a vacuum oven prior to further investigations. In our measurements, we have used probe needles made from beryllium copper, whereby the electrode material could have some influence on the electrochemical window due to irreversible electrode reactions at the reductive and oxidative limits. However, for all our measurements, we never exceeded $|V_{GS}| \leq 1.9$ V (typically ≤ 1.5 V) to stay within the electrochemical window as lower bound. Moreover, the overall device behavior did not change when sweeping up to 1.9 V compared to the 1.5 V sweeps, indicating that no irreversible electrochemical reactions take place. Transfer and output curves were measured at room temperature in a high vacuum using the wiring scheme in Fig. 1(d) using a Lakeshore CRX-VF probe station. A Yokogawa 7651 DC source was used to apply V_{DS} to the drain electrode. To allow for highly accurate current determination, the drain current I_D was measured using a current preamplifier (1211 DL Instruments) and an HP 34401 A voltage meter. For the gate voltage V_{GS} and gate current I_G, a Keithley 2450 was used. The charge transport calculations are based on the Landauer–Büttiker formalism,[33] and consider assumptions for the band alignment, doping, temperature, and gate control imperfection due to quantum capacitance. The code has been implemented in python, and the main code, as well as the input functions and parameters, is available online.[34] The simulation model allows simple and quick calculations by considering a perfect ballistic nanotube, where losses occur only at the CNT/electrode contacts.

The electrolyte gated CNT transistors typically show on-off ratios up to 10^4, a subthreshold swing down to 100 mV/dec, and a maximum diameter-normalized current density of 2.57 mA/μm. The latter value slightly outperforms 2.41 mA/μm[4] of a solid gated CNT transistor with similar device dimensions at the same source-drain voltage of -0.5 V, which demonstrates the high quality of our devices. We have measured various devices that are labeled with #1–3 for a channel length of 20 nm and #4–5 for a channel length of 10 nm. Output and transfer characteristics of a 20 nm channel length CNT transistor (device #1) are given in Fig. 2 for negative V_{DS} (a) and (b) and positive V_{DS} (c) and (d). The transfer curves for all devices exhibit ambipolar transport for electrons and holes. Despite the short channel length of 20 nm, only small short channel effects were observable: For one, at small V_{GS}, the output curves exhibit a non-ideal saturation of the drain current I_D. Second, in the transfer characteristics, a slight V_{DS}-dependent shift of the threshold voltage V_{th}, which is related to drain-induced barrier lowering,[35] could be measured. The current

plateaus in Fig. 2(b) for $V_{GS} < 0$ can be associated with contributions of the second band, as will be explained in the theory section. Even devices with a channel length of only 10 nm show almost ideal electrical device characteristics with a complete saturation in the output current, well-defined off and on regime in the transfer curves with a steep subthreshold slope (see the supplementary material, Fig. 1, device #5). The absence of noteworthy short channel effects can be explained by the high capacity and, hence, large gate coupling of the ionic liquid that allows for an almost complete control of the charge carrier density throughout the CNT.[36] The best measured subthreshold swing for a 10 nm channel length transistor (see the supplementary material, Fig. 2 device #4) was 100 mV/dec, which compares well with 94 mV/dec of solid-state gated short–channel FETs ($L_{ch} = 9$ nm)[4] and again underlies the excellent electrical parameters of our devices. A more detailed comparison between this work and literature can be found in the supplementary material, Table 1.

It is noticeable in all our transistors that the transfer curves are shifted to positive gate values, which indicates p-doping of our transistors. We consequently have analyzed the threshold voltage in greater detail to find the cause of the p-doping. Since the extraction of V_{th} for small V_{DS} in the p-branch for negative V_{GS} of the transfer characteristics is delicate due to different slopes with intermediate plateaus [see Figs. 2(b) and 2(d)], we focus on $V_{DS} = -0.5$ V. The V_{th} values in our measurements are 0.2 V [device #1, Fig. 2(b)], 0.22 V [device #2, Fig. 3(a)], and 0.28 V [device #3, supplementary Fig. S3(d)]. An overview of all V_{th} values can be found in the supplementary material, Table 2. In the literature, two main physical reasons for p-type doping are discussed. For one, metal-induced p-doping at the SWCNT/Pd electrode interface[37,38] has been observed for short channel lengths down to 9 nm.[39] However, the p-doping due to the Pd electrode is not expected as large in our FETs as in traditional CNT-FETs, where the tube is usually embedded into metal electrodes. In contrast, in our devices, the tubes lie on top of the contacts[40] and are potentially additionally protected from contact metal-induced doping by the polymer wrapping around the CNTs. While we cannot exclude contact-induced doping altogether, we anticipate that a second scenario dominates in these particular measurements, the p-doping, namely, residual oxygen dissolved in the CNT's surrounding ionic liquid. The physical reasons for p-doping of oxygen can be a modification of the barrier height at the semiconductor metal interface[41] or that oxygen adsorbates act as electron trap states (thus leading to hole doping) since the LUMO of oxygen lies in between the CNT's bandgap.[42] Also, a combination of both effects has been shown to be possible.[43]

To investigate the influence of residual oxygen and water on the electrical device characteristics in further detail, we performed additional measurements while keeping the samples in vacuum (see the supplementary material, Fig. 3). The initial measurements (which were discussed until now) were conducted in the first two days after loading the samples into the chamber at a pressure of $6.2 - 2.5 \times 10^{-5}$ mbar. After storing the samples in vacuum for more than two weeks, the pressure had dropped to 1×10^{-5} mbar and we performed a second measurement. In this second measurement (again measured at $V_{DS} = -0.5$V), V_{th} decreases for all three devices both in the p-branch for negative V_{GS} and in the n-branch for positive V_{GS} (see the supplementary material, Table 2). This effect becomes particularly obvious by applying positive V_{DS} in device #1, whereby V_{th} decreases about 0.15 V–0.18 V for different V_{DS} values (see the supplementary material
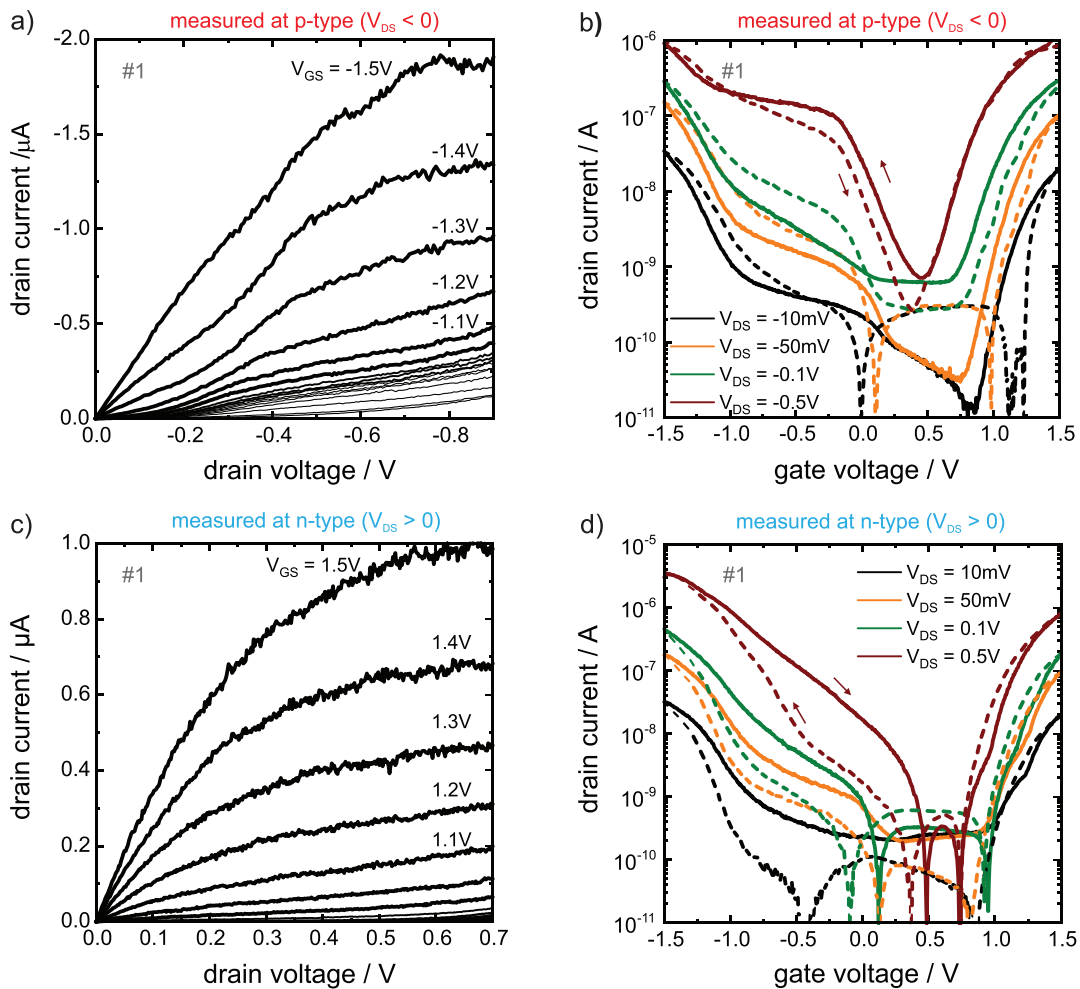
FIG. 2. Electrical transport measurements of the (9, 8) carbon nanotube device (#1) with a channel length of 20 nm under ionic liquid gating measured within two days after loading the sample in the vacuum setup at a pressure of $6.2 - 2.5 \times 10^{-5}$ mbar. (a-b) P-type and (c) and (d) n-type transfer and output characteristics measured at a V_{GS} sweep rate of 26 mV s^{-1} (solid lines: forward sweep; dashed lines: backward sweep). Gate voltages (V_{GS}) and Source-drain voltages (V_{DS}) are indicated. For the measurements in (b) (d), we started the gate sweep at $V_{GS} = +1.5$ V ($V_{GS} = -1.5$ V).

Fig. 4 and supplementary material Table 3). These results indicate oxygen to be the main reason for the initial strong p-doping (as previously reported[41–43]) instead of metal-induced p-doping since in this case, the threshold voltage should not be affected by different pressures. It has to be mentioned that water molecules cannot fully excluded to be the reason for the initial p-doping. However, we could not find conclusive evidence in the literature for this argument.

A further non-ideality of our devices is the hysteresis between forward and backward sweep in the transfer characteristics. Hysteretic behavior in nanoscale transistors is well-known,[44,45] and the higher back sweep current hysteresis [see Fig. 2(b)] can be explained by a slow polarization change in the ionic liquid caused by the diffusion of mobile ions in the liquid electrolyte.[10,46,47] Note that the measurements conducted in Fig. 2(b) were performed as p-type, i.e., starting at +1.5 V V_{GS}, and it follows that, e.g., for $V_{DS} = -10$ mV, for both hole and electron conduction, the current is larger upon tuning the Fermi

level toward the bandgap (i.e., on both p- and n-sides, the current is larger upon tuning that particular conduction channel off). We also find for measurements in the p-mode [also compare Fig. S1(b)] that for high V_{DS}, the direction of the hysteresis for hole conduction reverses. We anticipate that the reason is that for increasing V_{DS}, the total current increases, and hence, more charge carriers can be trapped. Charge trapping (potentially by residual water[44] or oxygen molecules around the nanotube[42,43]) dominates the slow polarization effect of the ionic liquid, which results in a lower back sweep current hysteresis for $V_{DS} = -0.5$ V [see Figs. 2(b), 3(a), and supplementary material Figs. S1(b) and S3(d)]. In the second measurement performed after the devices had been stored in vacuum for more than two weeks, the counterclockwise hysteresis is reduced consistent with a reduction in the water and oxygen concentration, as also put forward in the literature previously[44,45] [see the supplementary material, Fig. S3(d) again for high V_{DS}]. The remaining small hysteresis might be due to residual
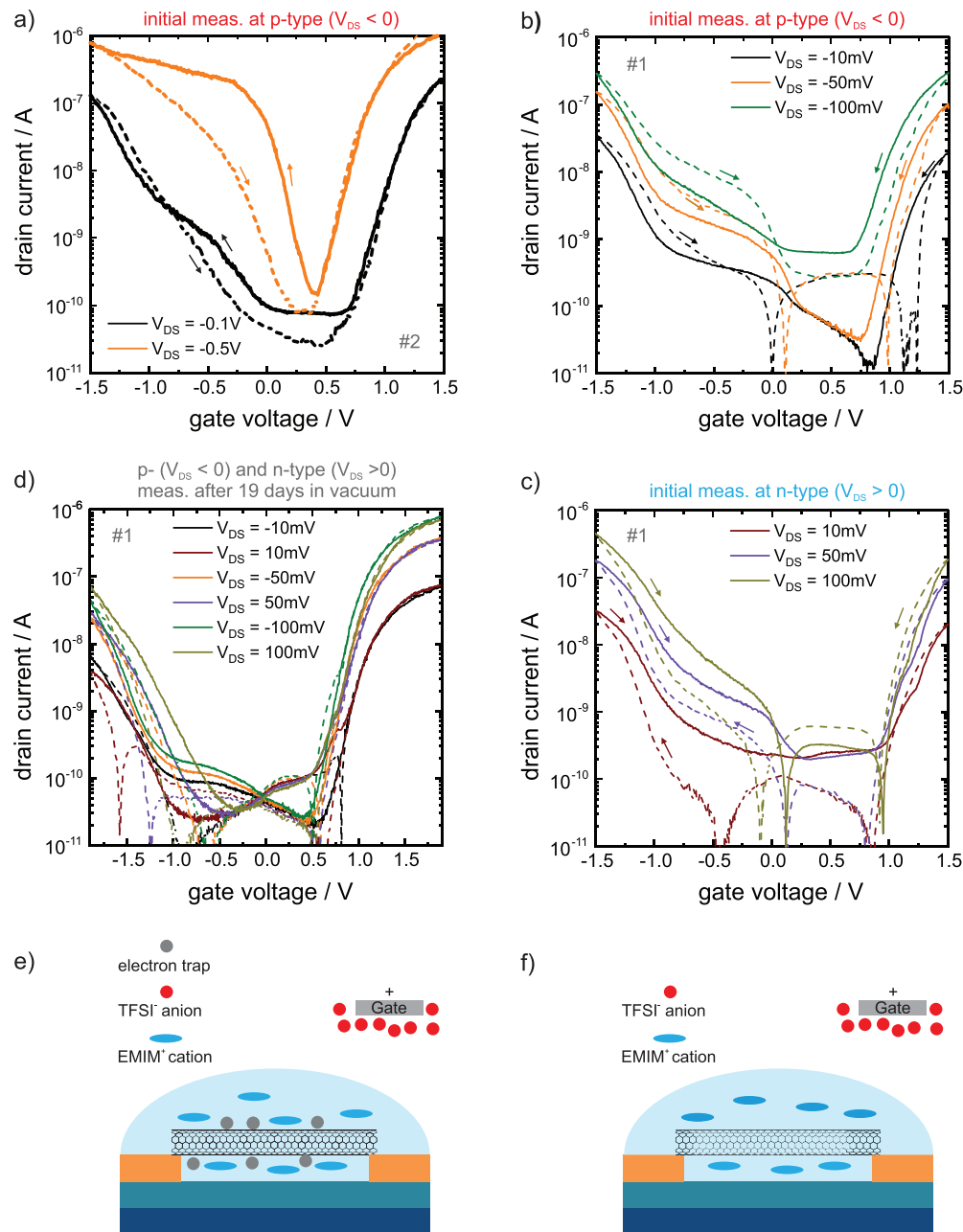
FIG. 3. P-type transfer characteristic of (a) device #2 ($p = 5.4 \times 10^{-5}$ mbar, measured within two days after loading the sample in the vacuum setup) with $L_{ch} = 20$ nm. (b) and (c) first measured ($p = 2.5 \times 10^{-5}$ mbar and V_{GS} sweep rate, 26 mV s^{-1}) p- and n-type transfer characteristics of device #1. (d) P- and n-type transfer characteristics of the same device after storing the sample in vacuum ($p = 1 \times 10^{-5}$ mbar and V_{GS} sweep rate 10 mV s^{-1}). (e) Schematic illustration of the higher pressure first measurement with electron traps (oxygen and water) in the vicinity of the nanotube, which attracts the EMIM$^+$ cation of the ionic liquid. (f) Analog scenario with reduced traps after storing the sample in vacuum for the lower pressure second measurement. With less trapped electrons and, hence, less attracted cations, the hysteresis decreases.

water still present in high vacuum, as recently shown by Kettner et al.,[48] and due to the still existing slow polarization effect. We have found a further interesting point upon measuring the devices for small V_{DS} ($|V_{DS}| = 10$, 50, and 100 mV), which had a smaller water and oxygen content {for most devices, this was the case after storage for

two weeks in vacuum [Fig. 3(d)], and others apparently were cleaner and showed this effect immediately [e.g., Fig. 3(a)]}. The effect can be seen clearer in the devices presented in Figs. 3(b)–3(d) for the electron branch (positive gate-source voltages). While after directly loading the devices [Figs. 3(b) and 3(c)] on the electron side, a higher current back
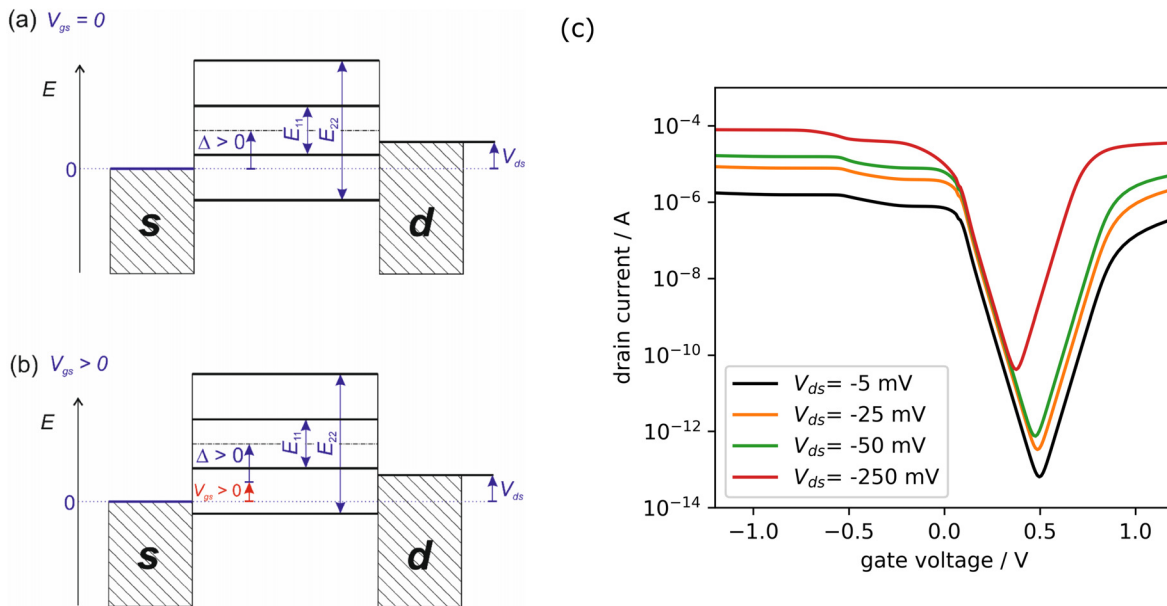
FIG. 4. Simulations (a) and (b) band alignment of the carbon nanotube with respect to the source (s) and drain (d) contact, with the energy difference E_{11} and E_{22} of the first and second pair of bands, the doping parameter Δ, source-drain voltage V_{DS}, and gate voltage V_{GS}. (c) Calculated transfer characteristic for a (9,8) carbon nanotube using the Landauer–Büttiker formalism with parameters $E_{11} = 0.879\,eV$, $E_{22} = 1.533\,eV$, $\Delta = 0.5\,eV$, $T = 300\,K$, screening length $l = 1.7\,nm$, and dielectric permittivity of the ionic liquid $\epsilon = 12$.

gate hysteresis could be seen (consistent with the slow polarization dynamics of the ionic liquid), after two weeks in vacuum, all hysteresis for $V_{GS} > 0$ has vanished [see Fig. 3(d)]. This is surprising at first sight since *a priori* one might anticipate that the polarization dynamics of the ionic liquid is not dependent on the residual water content and should affect both $V_{GS} < 0$ and $V_{GS} > 0$ branches similarly. One can explain the effect, however, as schematically shown in Fig. 3(e), by anticipating that oxygen and water in the vicinity of the tube trap electrons, which, in turn, then attract cations from the ionic liquid. These trapped cations remain longer in the vicinity of the tube, thus leading to the higher current back sweep hysteresis for $V_{GS} > 0$. While it is well established that oxygen molecules can act as electron trap states,[42,43] it has been shown that water molecules can trap both electrons[49] and holes.[50] We can only speculate why for ionic liquid gated CNT transistors, water tends to trap predominantly electrons. If the number of trap states is reduced, the cations become more mobile, and hence, the hysteresis reduces. We, thus, believe that this is a hysteresis mechanism for ionic liquid gating, which is relevant at the slow sweeping frequencies that we have used and complements the usually found hysteresis mechanism of ionic liquids at higher frequencies. As a consequence, for the same sweep rate of $10\,mV\,s^{-1}$, forward and backward sweeps for positive V_{GS} are almost identical in Fig. 3(d), whereas the hysteresis remains observable for negative V_{GS}.

The influence of oxygen and water is further underlined by comparing the electron and hole conduction branches between the first and second measurements. Supplementary material Figs. S3 and 3(b)–3(d) show that in the second measurement (i.e., after devices had been stored in vacuum for more than two weeks), I_{on} in the p-branch decreases, while I_{on} in the n-branch increases. This effect has been widely

discussed[41–43] and can be explained by a reduction in the oxygen concentration in vacuum with a subsequent reduction in the injection barrier for electrons at the contacts. The superior electron conduction in the second measurement in Fig. 3(d) in the absence of hysteresis and almost identical curves for positive and negative V_{DS} for $V_{GS} > 0$ indicates nearly ideal electron transport characteristics without external influences.

After discussing the non-idealities in the electrical characteristics, we now try to obtain possible experimental knowledge for device improvement by performing the charge transport calculation based on the model developed on the basis of Landauer–Büttiker (LB) formalism for a ballistic carbon nanotube as described in the supplementary material, Sec. S1. The effect of the quantum capacitance has been taken into account, as described in the supplementary material, Sec. S2. The main code, input functions, and all parameters are available in a repository.[34]

Having computed both quantum and electrostatic capacitances, we have found that for a given ionic liquid (dielectric permittivity $\epsilon = 12$ and[51] screening length $l = 1.7\,nm$[52]) the quantum capacitance has the same order of magnitude as the electrostatics gate capacity and, thus, cannot be neglected. Figures 4(a) and 4(b) illustrate the CNT's band alignment for zero V_{GS} and $V_{GS} > 0$. In the proposed model, the shift of the Fermi level due to p-doping is taken to be $0.5\,eV$, so that the Fermi level slightly penetrates the first valence energy band. This is consistent with Ref. 40, which shows that even for the on-top contact, the Fermi level lies slightly below the valence band edge. The p-type simulated data for varying V_{DS} values [see Fig. 4(c)] show V-shaped transfer characteristics and a threshold voltage shift to lower V_{GS} for increasing negative V_{DS}. Concerning the shape and structure of the curves in Figs. 2(b) and 3(a), the experiment and model are in qualitatively good agreement. The slight asymmetry in

the on-state current of the experimental data might be attributed to different Schottky barriers for electrons and holes, whereby the LB model assumes symmetric Ohmic contacts. At $V_{GS} \approx -0.25 \ldots -0.5$ V in Fig. 4(c), the current increases again after a first saddle point due to the contribution of the second band. The increase in the current occurs steadily, because of the quantum capacitance (see the supplementary material, Fig. S8). A saddle point with a subsequent increase in the current can also be seen in the experimental data in Fig. 2(b).

Both experimental and simulation data feature ambipolar transfer characteristics, which is explained by a strong gate control due to a liquid gate. As shown in Fig. S8 of the supplementary material, the effect of the quantum capacitance does not affect the magnitude of the subthreshold swing. An experimentally observed SS value of 100 mV/dec (vs theoretical 60 mV/dec) has to be, thus, related to the residual polymer (PFD), short-channel effects, and other factors.

Except for the high drain-source voltage, the experimental data demonstrate a diverse shape of the transfer curve, while the model always predicts V-shaped characteristics. This cannot be explained by internal nanotube properties and is not captured by a proposed model. We may speculate that it may be caused by shallow charge traps, where de-trapping requires higher drain-source voltages.

Another important discrepancy between the model and the experiment is the difference in the on-current, which reaches two orders of magnitudes. As far as the tube contacts are p-type doped, we expect no Ohmic barriers at least for the p-branch. The current reduction can, thus, be primarily related to the effect of the polymer wrapping, which may increase an effective distance between the tube and the metallic electrode; this may be critical in on-top geometry where orbitals of the metal only overlap with a few bottom C atoms of the tube. As a result of these two effects, despite a considerable overlap ($\sim$100 nm contact length), the tube may still be unable to accept all the current from the metal. In Ref. 40, it has been shown that the necessary contact length quickly increases as the coverage of the tube by the metal decreases. The expected increase in the tube-metal separation due to the residual polymer would facilitate this effect greatly, as the orbital overlap drops exponentially with the interatomic distance.

In summary, we have shown high-performance nanoscopic SWCNT transistors in which the use of an electrolyte gate allows efficient control of the electrostatics in the nanoscopic channel even though the channel is made as short as 10 nm. Our transistors show a small subthreshold swing down to 100 mV/dec and diameter-normalized current densities as high as 2.6 mA/μm, which is comparable to all-solid-state short-channel SWCNT transistors.[4] Whereas a higher current back sweep hysteresis in ionic liquids usually is attributed to the ion dynamics in the ionic liquid itself, we have identified that electron trapping can also lead to the same type of hysteresis. The favorable device characteristics allow good comparison with the developed model based on Landauer–Büttiker formalism, including the effect of the quantum capacitance. Based on this model, the theoretically reachable performance of fabricated devices has been estimated, and the experimental data have been validated. From the simulations, we can deduce that a reduction of traps influencing the subthreshold slope and the better contact between the SWCNTs and the metal will improve the device characteristics even further.

See the supplementary material for additional electrical measurements and details on the simulation.

DATA AVAILABLITITY

The data that support the findings of this study are either available from the corresponding author upon reasonable request or available in GitHub repository, Ref. 34.

REFERENCES

[1] S. J. Tans, A. R. M. Verschueren, and C. Dekker, Nature **393**, 49 (1998).
[2] Nat. Electron. **1**, 149 (2018).
[3] G. Hills, C. Lau, A. Wright, S. Fuller, M. D. Bishop, T. Srimani, P. Kanhaiya, R. Ho, A. Amer, Y. Stein, D. Murphy, Arvind, A. Chandrakasan, and M. M. Shulaker, Nature **572**, 595 (2019).
[4] A. D. Franklin, M. Luisier, S.-J. Han, G. Tulevski, C. M. Breslin, L. Gignac, M. S. Lundstrom, and W. Haensch, Nano Lett. **12**, 758 (2012).
[5] Q. Cao, S.-J. Han, J. Tersoff, A. D. Franklin, Y. Zhu, Z. Zhang, G. S. Tulevski, J. Tang, and W. Haensch, Science **350**, 68 (2015).
[6] R. Misra, M. McCarthy, and A. F. Hebard, Appl. Phys. Lett. **90**, 052905 (2007).
[7] S. Ono, S. Seki, R. Hirahara, Y. Tominari, and J. Takeya, Appl. Phys. Lett. **92**, 103313 (2008).
[8] M. Kettner, I. Vladimirov, A. J. Strudwick, M. G. Schwab, and R. T. Weitz, J. Appl. Phys. **118**, 025501 (2015).
[9] J. Lee, L. G. Kaake, J. H. Cho, X.-Y. Zhu, T. P. Lodge, and C. D. Frisbie, J. Phys. Chem. C **113**, 8972 (2009).
[10] S. H. Kim, K. Hong, W. Xie, K. H. Lee, S. Zhang, T. P. Lodge, and C. D. Frisbie, Adv. Mater. **25**, 1822 (2013).
[11] C. Rutherglen, A. A. Kane, P. F. Marsh, T. A. Cain, B. I. Hassan, M. R. AlShareef, C. Zhou, and K. Galatsis, Nat. Electron. **2**, 530 (2019).
[12] M. Steiner, M. Engel, Y.-M. Lin, Y. Wu, K. Jenkins, D. B. Farmer, J. J. Humes, N. L. Yoder, J.-W. T. Seo, A. A. Green, M. C. Hersam, R. Krupke, and P. Avouris, Appl. Phys. Lett. **101**, 053123 (2012).
[13] J. Lenz, F. Del Giudice, F. R. Geisenhof, F. Winterer, and R. T. Weitz, Nat. Nanotechnol. **14**, 579 (2019).
[14] S. Joshi, V. D. Bhatt, E. Jaworska, A. Michalska, K. Maksymiuk, M. Becerer, A. Gagliardi, and P. Lugli, Sci. Rep. **8**, 11386 (2018).
[15] K. Kim, C.-L. Chen, Q. Truong, A. M. Shen, and Y. Chen, Adv. Mater. **25**, 1693 (2013).
[16] A. B. Artyukhin, M. Stadermann, R. W. Friddle, P. Stroeve, O. Bakajin, and A. Noy, Nano Lett. **6**, 2080 (2006).
[17] S. Rosenblatt, Y. Yaish, J. Park, J. Gore, V. Sazonova, and P. L. McEuen, Nano Lett. **2**, 869 (2002).
[18] J. H. Back and M. Shim, J. Phys. Chem. B **110**, 23736 (2006).

[19]G. P. Siddons, D. Merchin, J. H. Back, J. K. Jeong, and M. Shim, Nano Lett. **4**, 927 (2004).

[20]I. Heller, S. Chatoor, J. Männik, M. A. G. Zevenbergen, C. Dekker, and S. G. Lemay, J. Am. Chem. Soc. **132**, 17149 (2010).

[21]I. Heller, A. M. Janssens, J. Männik, E. D. Minot, S. G. Lemay, and C. Dekker, Nano Lett. **8**, 591 (2008).

[22]T. Sharf, N.-P. Wang, J. W. Kevek, M. A. Brown, H. Wilson, S. Heinze, and E. D. Minot, Nano Lett. **14**, 4925 (2014).

[23]J. Männik, I. Heller, A. M. Janssens, S. G. Lemay, and C. Dekker, Nano Lett. **8**, 685 (2008).

[24]F. Jakubka, S. B. Grimm, Y. Zakharko, F. Gannott, and J. Zaumseil, ACS Nano **8**, 8477 (2014).

[25]H. Wang, B. Wang, X.-Y. Quek, L. Wei, J. Zhao, L.-J. Li, M. B. Chan-Park, Y. Yang, and Y. Chen, J. Am. Chem. Soc. **132**, 16747 (2010).

[26]H. Wang, L. Wei, F. Ren, Q. Wang, L. D. Pfefferle, G. L. Haller, and Y. Chen, ACS Nano **7**, 614 (2013).

[27]M. Gaulke, A. Janissek, N. A. Peyyety, I. Alamgir, A. Riaz, S. Dehm, H. Li, U. Lemmer, B. S. Flavel, M. M. Kappes, F. Hennrich, L. Wei, Y. Chen, F. Pyatkov, and R. Krupke, ACS Nano **14**, 2709 (2020).

[28]A. Vijayaraghavan, S. Blatt, D. Weissenberger, M. Oron-Carl, F. Hennrich, D. Gerthsen, H. Hahn, and R. Krupke, Nano Lett. **7**, 1556 (2007).

[29]M. Engel, M. Steiner, R. S. Sundaram, R. Krupke, A. A. Green, M. C. Hersam, and P. Avouris, ACS Nano **6**, 7303 (2012).

[30]U. Schröder, J. D. Wadhawan, R. G. Compton, F. Marken, P. A. Z. Suarez, C. S. Consorti, R. F. de Souza, and J. Dupont, New J. Chem. **24**, 1009 (2000).

[31]A. M. O'Mahony, D. S. Silvester, L. Aldous, C. Hardacre, and R. G. Compton, J. Chem. Eng. Data **53**, 2884 (2008).

[32]M. Hayyan, F. S. Mjalli, M. A. Hashim, I. M. AlNashef, and T. X. Mei, J. Ind. Eng. Chem. **19**, 106 (2013).

[33]R. Landauer, IBM J. Res. Develop. **1**, 223 (1957).

[34]A. Fediai, *LiquidGate: A Python-Based Software to Simulate Current-Voltage Characteristics of the CNTFET With Liquid Gating*, GItHub Repository, https://github.com/ArtemFediai/LiquidGate.

[35]K. Roy, S. Mukhopadhyay, and H. Mahmoodi-Meimand, Proc. IEEE **91**, 305 (2003).

[36]L. Herlogsson, Y. Y. Noh, N. Zhao, X. Crispin, H. Sirringhaus, and M. Berggren, Adv. Mater. **20**, 4708 (2008).

[37]A. Fediai, D. A. Ryndyk, and G. Cuniberti, Phys. Rev. B **91**, 165404 (2015).

[38]A. Fediai, D. A. Ryndyk, G. Seifert, S. Mothes, M. Claus, M. Schröter, and G. Cuniberti, Nanoscale **8**, 10240 (2016).

[39]A. Fediai, D. Ryndyk, and G. Cuniberti, in Contact Properties of Ultrasmall Carbon Nanotube Transistors from Ab-Initio, *Kyiv, Ukraine, 15–18 April 2014* (IEEE, Piscataway, NJ, 2014).

[40]A. Fediai, D. A. Ryndyk, G. Seifert, S. Mothes, M. Schroter, M. Claus, and G. Cuniberti, Appl. Phys. Lett. **109**, 103101 (2016).

[41]V. Derycke, R. Martel, J. Appenzeller, and P. Avouris, Appl. Phys. Lett. **80**, 2773 (2002).

[42]D. Kang, N. Park, J. Hyun, E. Bae, J. Ko, J. Kim, and W. Park, Appl. Phys. Lett. **86**, 093105 (2005).

[43]D. McClain, N. Thomas, S. Youkey, R. Schaller, J. Jiao, and K. P. O'Brien, Carbon **47**, 1493 (2009).

[44]W. Kim, A. Javey, O. Vermesh, Q. Wang, Y. Li, and H. Dai, Nano Lett. **3**, 193 (2003).

[45]R. T. Weitz, U. Zschieschang, F. Effenberger, H. Klauk, M. Burghard, and K. Kern, Nano Lett. **7**, 22 (2007).

[46]M. Egginger, S. Bauer, R. Schwödiauer, H. Neugebauer, and N. S. Sariciftci, Monatsh. Chem. **140**, 735 (2009).

[47]J. H. Cho, J. Lee, Y. He, B. S. Kim, T. P. Lodge, and C. D. Frisbie, Adv. Mater. **20**, 686 (2008).

[48]M. Kettner, M. Zhou, J. Brill, P. W. M. Blom, and R. T. Weitz, ACS Appl. Mater. Interfaces **10**, 35449 (2018).

[49]H. T. Nicolai, M. Kuik, G. A. H. Wetzelaer, B. de Boer, C. Campbell, C. Risko, J. L. Brédas, and P. W. M. Blom, Nat. Mater. **11**, 882 (2012).

[50]M. Nikolka, I. Nasrallah, B. Rose, M. K. Ravva, K. Broch, A. Sadhanala, D. Harkin, J. Charmet, M. Hurhangee, A. Brown, S. Illig, P. Too, J. Jongman, I. McCulloch, J.-L. Bredas, and H. Sirringhaus, Nat. Mater. **16**, 356 (2017).

[51]M.-M. Huang, Y. Jiang, P. Sasisanker, G. W. Driver, and H. Weingärtner, J. Chem. Eng. Data **56**, 1494 (2011).

[52]M. Jitvisate and J. R. T. Seddon, J. Phys. Chem. Lett. **9**, 126 (2018).